

Application of harmonic and anharmonic frequency crystals for manipulation with quantum states

R. N. Shakhmuratov

*Zavoisky Physical-Technical Institute, FRC Kazan Scientific Center of RAS, Kazan 420029, Russia
and Institute of Physics, Kazan Federal University, 18 Kremlyovskaya Street, Kazan 420008, Russia*

(Received 26 April 2018; published 29 October 2018)

Filtering of weak pulses through a medium with infinite periodic structure in the absorption and/or transmission spectrum is analyzed. Two types of filters are considered. The first, named harmonic frequency crystal (HFC), is the filter whose periodic structure is harmonic and described by the sine or cosine function of frequency with the fundamental period. The second, named anharmonic frequency crystal (AHFC), also has a periodic structure with one fundamental period but it is described by the function containing many harmonics of the fundamental period. AHFC demonstrates properties quite similar to those of a high-finesse atomic frequency comb (AFC) with a limited number of absorption peaks separated by transparency windows. Filtering of the pulse through AHFC produces a prompt pulse accompanied by a few delayed pulses. Time spacing T of the delayed pulses is inversely proportional to the comb period. On the contrary, HFC transforms the input pulse into a train of many delayed pulses, generated at times nT , where n is an integer. Maximum amplitudes of the delayed pulses follow a wide bell-shaped envelope. Both HFC and AHFC are extensions of AFC, which was proposed to implement quantum memory protocols for single photons. In this paper, it is proposed to create time-bin qubits with the help of a short pulse filtering through HFC. HFC is also proposed to implement tomography of these quantum states. Another promising application of HFC is the optical detection of ultrasound in biological tissues for ultrasound-modulated optical tomography. Since HFC allows one to generate pulses with longer delay with respect to the excitation pulse, one could obtain higher discrimination between weak acoustically generated sidebands and the carrier.

DOI: [10.1103/PhysRevA.98.043851](https://doi.org/10.1103/PhysRevA.98.043851)**I. INTRODUCTION**

Infinite periodical structures in space, time, and frequency are models, which allow simple analytical solutions. Ideal crystals infinite in space are nice models to predict electron, phonon, and thermodynamical properties of real crystals. A time crystal or space-time crystal, which is a structure that repeats in time as well as in space, recently was proposed to create objects with unusual thermodynamical properties never reaching thermal equilibrium [1–7]. Frequency crystals with a periodic structure in the absorption spectrum of the electromagnetic field were proposed as a quantum memory for repeaters [8–12]. These crystals were not ideal since they have finite length in a frequency domain with decreasing depths of the transparency windows at the edges of the spectrum. They were created in an inhomogeneously broadened absorption spectrum of crystals with rare-earth-metal impurity ions by the spectral hole-burning technique. Therefore, these frequency crystals were named atomic frequency combs (AFCs).

In this paper, the ideal crystals are considered with infinite periodic structure of transparent holes in the absorption spectrum. The sequence of transmission and absorption windows follows harmonic law and can be described by the sine function. Therefore, the absorber with such a structure can be named harmonic frequency crystal (HFC). The harmonicity allows one to derive an exact solution with a very simple structure, which discloses the physical properties of the generated pulses at the exit of the HFC. In contrast to an AFC, a HFC generates a series of pulses whose maximum amplitudes build

a bell-shaped envelope with much longer duration than the interval T between pulses, which is the inverse value of the frequency period of the comb. Numerical simulations confirm the validity of the exact solution. It should be noted that an infinite spectrum of the HFC is necessary only for derivation of the solution, while the result perfectly describes the case if one truncates in numerical simulations the spectrum of the HFC to finite boundaries where the pulse spectrum has noticeable power.

A HFC has a remarkable potential to create time-bin qubits, which are single-photon quantum states. Single photons are ideal information carriers for quantum communication and computing. In the vast majority of quantum protocols, photon polarization is used as the information carrier [13]. Time-bin qubits, proposed and implemented in Refs. [14,15], were practically the first examples of how the time domain can be involved in the information coding by splitting a single photon into two pulses with a fixed phase difference and controllable amplitudes. The information carried by such a photon is well protected during its propagation in optical fiber since cross talk, which usually influences the polarization states of a photon, is excluded. Time coding of information is implemented in [14,15] by the unbalanced interferometer having different lengths of the arms and a phase shifter placed in the long arm. Unbalanced three-path interferometers were used in [16] to create three-state quantum objects (qutrits). Recently, new methods to process time-bin qubits [17,18] and to create time-bin qubits, qutrits, and ququads [19] were reported.

In this paper, we propose to create time-bin qubits by filtering a weak short pulse through the HFC. By shifting the carrier frequency of the pulse with respect to the central frequency of the HFC, it is possible to introduce a phase shift of the pulses growing with the number of the delayed pulse. This phase shift can be detected by transmitting the train of the delayed pulses through the next HFC with the shifted central frequency of the periodic spectrum. Instead of the second HFC, one can use only one HFC transmitting the pulse train in a backward direction through the same HFC by placing a mirror at its exit and shifting in a controllable way the carrier frequency of the pulses using an acousto-optic modulator (AOM). For a particular frequency shift, the amplitudes of the delayed pulses are exactly zero. The contrast between the intensity of the delayed pulses and the case when they collapse is incredible. This opens a way for tomography of the states generated by HFC.

Results for HFC are compared with numerical simulations and analytical calculations for anharmonic frequency combs (AHFCs). Two examples are considered. In one, the transmission windows follow the law $\sin^{10}(\pi v/2\nu_0)$, where $\nu = \omega_c - \omega$ is the frequency difference between the central frequency of the light pulse ω_c and its spectral component ω , and ν_0 is the distance from the center of the transmission window and the nearest absorption peak. The second example is a sequence of Lorentzian absorption peaks whose width could be much smaller than the distance between them. Such a structure is equivalent to an AFC with high finesse [8–12]. It is shown that an AHFC demonstrates large contrast in the tomography protocol if we detect photons in a predefined short-time window.

Recently, the transformation of a long pulse with a comb spectrum into a train of coherent short pulses by filtering through a single-narrow-line absorber was proposed and experimentally implemented with single γ photons [20–22]. In this paper, the transformation of a short pulse into a long train of coherent pulses by filtering through a comb structure is proposed.

Another promising application of the HFC is optical detection of ultrasound in biological tissues for ultrasound-modulated optical tomography. It was shown that the AFC allows high discrimination between the sidebands and the carrier [23,24]. The carrier is split into sidebands by ultrasound modulation in a biological tissue. The scattered light is transmitted through a filter with a broad transparent dip in its spectrum for the carrier and two AFCs for the generated sidebands. They are delayed in time with respect to the carrier, which leads to high discrimination (about 49 dB) of the central frequency with respect to the sidebands. One could expect that the HFC could appreciably increase this discrimination due to the lengthening of the delay time and consequent increase of the signal-to-noise ratio.

The paper is organized as follows. In Sec. II, the definition of the harmonic frequency crystal is introduced. With the help of Kramers-Kronig relation, the transmission function of the HFC is derived. In Sec. III, an exact solution for the pulse propagating in the HFC is obtained. The properties of the exact solution are discussed in Sec. IV. The application of the HFC to generate time-bin qubits is discussed in Sec. V. The properties of the anharmonic frequency combs are dis-

cussed in Secs. VI and VII. Their application for tomography of time-bin qubits is discussed in Sec. VIII. The results are discussed and summarized in Secs. IX and X.

II. HARMONIC FREQUENCY CRYSTAL

We start with a very general consideration of the propagation of a radiation pulse through a medium whose response is described by

$$\mathbf{P} = \varepsilon_0 \chi \mathbf{E}, \quad (1)$$

where \mathbf{E} is an electric field, \mathbf{P} is polarization density, ε_0 is the electric permittivity of free space (below we set $\varepsilon_0 = 1$ for simplicity), and χ is the electric susceptibility, which is

$$\chi = \chi' + i\chi''. \quad (2)$$

The imaginary part of susceptibility χ'' describes the field absorption. We suppose that χ'' is a harmonic periodic function,

$$\chi''_h(\nu) = \frac{\chi_0}{2} \left[1 - \cos\left(\frac{\pi \nu}{\nu_0}\right) \right], \quad (3)$$

which is infinite in frequency space. Here, index h means harmonic, χ_0 is the value, which depends on the interaction constant with the medium and its density, and $\nu = \omega_c - \omega$ is the frequency difference between the central frequency of the light pulse ω_c and its spectral component ω .

Equation (3) describes a periodic structure of transmission windows and absorption peaks with a distance between centers of the transparency windows and nearest absorption peaks equal to ν_0 . The widths of the peaks and windows are equal the same value ν_0 . Meanwhile, finesse F of the comb structure, defined in Ref. [9] as the ratio of the distance between the absorption peaks Δ_a and the width of the individual peak w_a , i.e., $F = \Delta_a/w_a$, is equal to 2 for the harmonic frequency crystal since its parameters are $\Delta_a = 2\nu_0$ and $w_a = \nu_0$. The transmission windows of the HFC are ideal, i.e., there is no absorption at the window center.

The sequence of the absorption peaks and transmission windows (3) is similar to that, which is burnt in the inhomogeneously broadened absorption spectrum of atoms by the pulse pairs separated by time $T = 2\pi/\Delta_a = \pi/\nu_0$; see Ref. [25] and the Appendix. These pairs are repeated many times with a dwell time much longer than the homogeneous dephasing time T_2 . The transmission windows, created by such a pulse trains, are not ideal since the remnant absorption at their bottom is usually not zero.

To satisfy causality, the dispersion relations or, more generally, Kramers-Kronig relations must be fulfilled that describe the frequency dependence of the wave propagation and attenuation. According to them, the real part of the susceptibility, responsible for a group velocity dispersion, satisfies one of the Kramers-Kronig relations,

$$\chi'(\nu) = \frac{1}{\pi} \mathcal{P} \int_{-\infty}^{\infty} \frac{\chi''(\nu')}{\nu' - \nu} d\nu', \quad (4)$$

where \mathcal{P} denotes the Cauchy principal value. Calculating the integral, we obtain

$$\chi'_h(\nu) = \frac{\chi_0}{2} \sin\left(\frac{\pi \nu}{\nu_0}\right). \quad (5)$$

The unidirectional wave equation, describing the propagation of the plane-wave field $E(z, t) = E_0(z, t) \exp(-i\omega_c t + ikz)$ along axis \mathbf{z} (see, for example, Ref. [26]), is

$$\left(\frac{\partial}{\partial z} + \frac{n}{c} \frac{\partial}{\partial t} \right) E_0(z, t) = i \frac{2\pi\omega_c}{nc} P_0(z, t), \quad (6)$$

where $E_0(z, t)$ is the pulse envelope, k is the wave number, $P(z, t) = P_0(z, t) \exp(-i\omega_c t + ikz)$ is the polarization induced in the medium, and n is the index of refraction (below we set $n = 1$ for simplicity).

By the Fourier transform,

$$F(\nu) = \int_{-\infty}^{+\infty} f(t) e^{i\nu t} dt, \quad (7)$$

Eq. (6) is reduced to a one-dimensional differential equation, whose solution is (see Ref. [26])

$$E_0(z, \nu) = E_0(0, \nu) \exp \left\{ i\nu \frac{z}{c} - \frac{\alpha_p z}{2\chi_0} [\chi_h''(\nu) - i\chi_h'(\nu)] \right\}, \quad (8)$$

where $E_0(0, \nu) = E_{\text{in}}(\nu)$ is a spectral component of the field incident to the frequency crystal, and α_p is the Beer's law attenuation coefficient describing absorption of a monochromatic field tuned in resonance with one of the absorption peaks.

For the harmonic frequency crystal of physical length l , we have

$$E_0(l, \nu) = E_0(0, \nu) \exp \left\{ i\nu \frac{l}{c} - \frac{d_p}{4} + \frac{d_p}{4} e^{i\pi\nu/\nu_0} \right\}, \quad (9)$$

where $d_p = \alpha_p l$ is the absorption depth (optical thickness) of the medium for the monochromatic radiation field tuned in resonance with one of the absorption peaks. Below, for simplicity, we neglect small value $i\nu l/c$ in the exponent, which is responsible for the small delay due to the pulse traveling the distance l with a speed of light c ($t_d = l/c$).

We note that according to Eqs. (8) and (9), intensity $I_0(l, \nu) = |E_0(l, \nu)|^2$ of the monochromatic radiation field with a single frequency $\omega_c + \nu$ transmitted through a thick filter is described by the function $\mathcal{T}_{\text{int}}(\nu, l) = \exp[-\alpha_p l \chi_h''(\nu)/\chi_0]$, i.e., $I_0(l, \nu) = \mathcal{T}_{\text{int}}(\nu, l) I_0(0, \nu)$. This function is quite different from the harmonic absorption function $\chi_h''(\nu)$, which is defined for a single atom or a thin slice of the filter. With increase of the optical thickness $\alpha_p l$ of the filter, the transmission peaks narrow and absorption dips broaden; see Fig. 1.

III. EXACT SOLUTION

Infinite periodical structures in the absorption and dispersion, given by Eqs. (3) and (5), allow one to find an exact solution (ES), which simply follows from the Taylor series

$$e^{(d_p/4)e^{i\pi\nu/\nu_0}} = \sum_{k=0}^{+\infty} \frac{(d_p/4)^k}{k!} e^{ik\pi\nu/\nu_0}. \quad (10)$$

Then, the Fourier transform of the ES is

$$E_0(l, \nu) = E_{\text{in}}(\nu) e^{-d_p/4} \sum_{k=0}^{+\infty} \frac{(d_p/4)^k}{k!} e^{ik\pi\nu/\nu_0}. \quad (11)$$

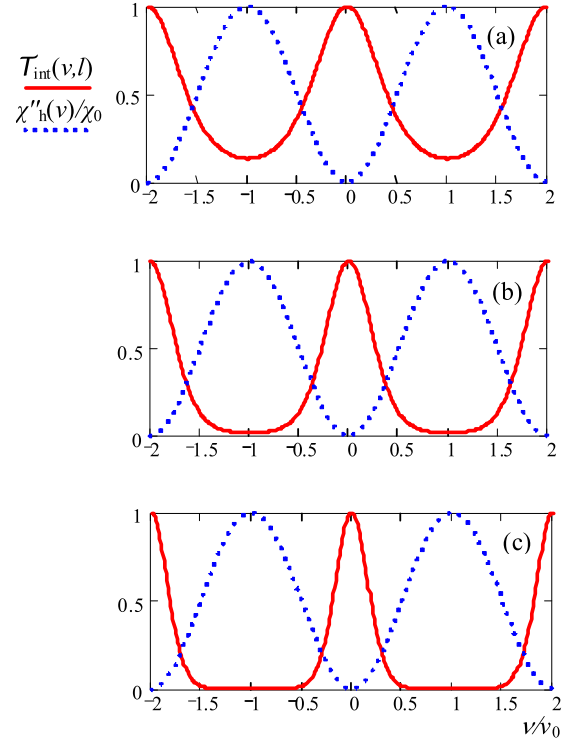


FIG. 1. Comparison of the frequency dependencies of the transmission function $\mathcal{T}_{\text{int}}(\nu, l)$ of the intensity of monochromatic radiation through the HFC (solid red line) and imaginary part of the susceptibility $\chi_h''(\nu)/\chi_0$ specifying the absorption by a single atom or a thin slice of the filter (dotted blue line). The optical thickness of the filter, $d_p = \alpha_p l$, is (a) 2, (b) 4, and (c) 8.

The inverse Fourier transformation of $E_0(l, \nu)$,

$$E_0(l, t) = \frac{1}{2\pi} \int_{-\infty}^{+\infty} E_0(l, \nu) e^{-i\nu t} dt, \quad (12)$$

gives the solution

$$E_{\text{out}}(t) = e^{-d_p/4} \sum_{k=0}^{+\infty} \frac{(d_p/4)^k}{k!} E_{\text{in}} \left(t - \frac{\pi k}{\nu_0} \right), \quad (13)$$

where $E_{\text{out}}(t) = E_0(l, t)$ is the field at the exit of the HFC. Pulse sequences, given by Eq. (13), generated at the exit of the HFC for different values of optical thickness d_p are shown in Fig. 2. For simplicity, as the input field, a pulse with a Gaussian envelope is taken, which is $E_{\text{in}}(t) = E_0 \exp(-r^2 t^2)$. Parameter r of the pulse is equal to $5\nu_0$, which means that the spectral width of the pulse covers more than ten absorption peaks. With increase of the optical thickness d_p of the absorption peaks, the line, which links maximum amplitudes of the pulses, generated at the exit of the crystal, forms a bell-shaped envelope, shown by the blue dotted line in Fig. 2(d). The time dependence of the envelope will be discussed in the next section.

The ES (13) is derived for the pulse whose central frequency ω_c is tuned in the center of one of the transparency windows. If there is a frequency shift δ_s of ω_c with respect to the transparency window center ω_{Tc} ($\omega_c = \omega_{Tc} - \delta_s$), the

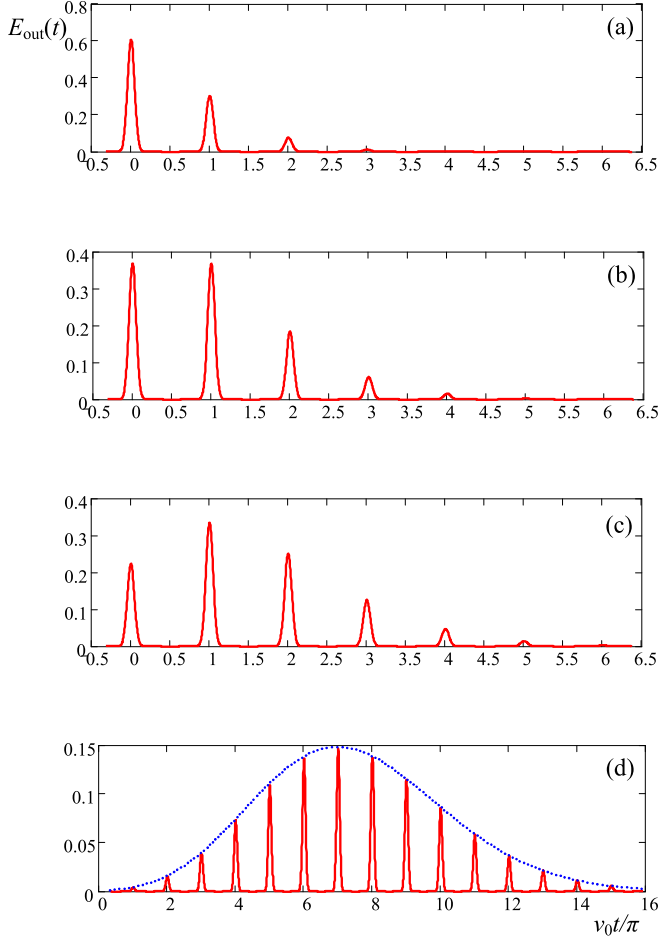


FIG. 2. Time dependence of the output field from the harmonic frequency crystals of different optical thickness d_p , which is (a) 2, (b) 4, (c) 6, and (d) 30. Timescale is in units of π/ν_0 and the field amplitude is normalized to the maximum amplitude $E_{in}(0)$ of the input pulse. The input pulse has a Gaussian shape, $E_{in}(t) = E_0 e^{-r^2 t^2}$, with $r = 5\nu_0$. The dotted blue line shows the net envelope of the pulse train, which is described by Eq. (25); see Sec. IV and discussion there.

solution (13) is modified as

$$E_{out}(t) = e^{-d_p/4} \sum_{k=0}^{+\infty} \frac{(d_p/4)^k}{k!} E_{in}\left(t - \frac{\pi k}{\nu_0}\right) e^{i\pi k \delta_s / \nu_0}. \quad (14)$$

When the central frequency of the pulse is tuned in resonance with one of the absorption peaks, for example, $\delta_s = \nu_0$, we have $\exp(i\pi k \delta_s / \nu_0) = \exp(i\pi k)$ and the pulses, generated at the exit of the HFC at times $t_k = \pi k / \nu_0$, have the phase opposite to the phase of the input pulse if k is odd; see Fig. 3(a).

The infinite spectrum of the frequency crystal is necessary only for the derivation of the exact solution. Below we show that the numerical solution, where the spectrum of the pulse, transformed by the crystal, is integrated in the limited domain, coincides with the ES. The numerical solution is obtained by

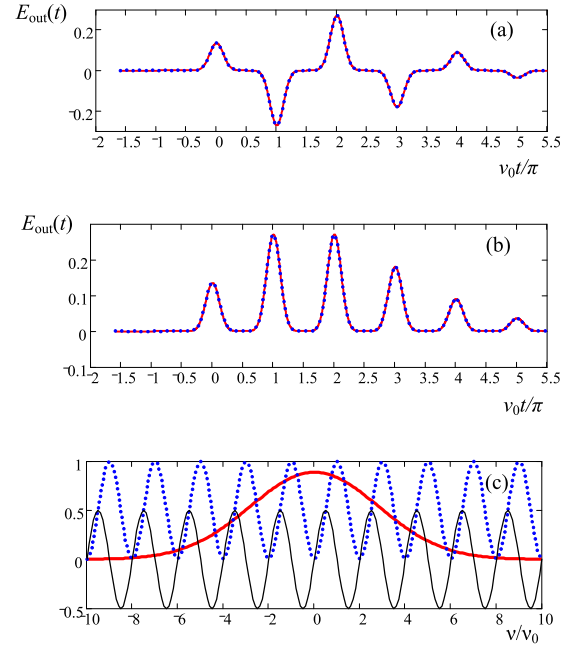


FIG. 3. Comparison of the exact solution (solid red line) with the numerical solution (blue dotted line), where the integration boundaries $\pm\Delta_b$ are limited by $\pm 10\nu_0$. The optical thickness of the absorption peaks is $d_p = 8$. The pulse central frequency is tuned (a) in one of the absorption peaks and (b) in the center of one of the transparency windows. Parameter r of the input pulse spectrum is equal to $2\nu_0$. The pulse amplitude is normalized to the amplitude of the input pulse E_0 . (c) Absorption $\chi''(\nu)$ and dispersion $\chi'(\nu)$ components of the HFC are shown by the dotted blue line and thin solid black line, respectively. Both are normalized to χ_0 . The input pulse spectrum (multiplied by ν_0 to make it dimensionless) is shown by a bold red line.

calculating the integral in the equation

$$E_{out}(t) = \frac{1}{2\pi} \int_{-\Delta_b}^{\Delta_b} E_{in}(\nu) e^{-i\nu t - (d_p/4)[1 \mp \cos(\pi \nu / \nu_0) \mp i \sin(\pi \nu / \nu_0)]} d\nu, \quad (15)$$

where $E_{in}(\nu)$ is the spectrum of the input pulse, Δ_b and $-\Delta_b$ are the boundaries of the numerical integration, and the \mp signs in the exponent correspond to tuning the central frequency of the pulse in the center of one of the transparency windows (sign minus) or in the center of one of the absorption peaks (sign plus). A comparison of the exact solution with the numerical results is shown in Figs. 3(a) and 3(b) for the Gaussian pulse $E_{in}(t) = E_0 \exp(-r^2 t^2)$ whose spectrum is $E_{in}(\nu) = (\sqrt{\pi}/r) E_0 \exp(-\nu^2/4r^2)$. Parameter r is taken equal to $2\nu_0$. Integration boundaries ($\pm\Delta_b = \pm 10\nu_0$) include the contribution of 10 absorption peaks; see Fig. 3(c).

IV. PROPERTIES OF THE EXACT SOLUTION

According to the exact solution (13), the maximum intensity of the pulse, transmitted through the HFC with no delay, $I_{out}(0) = |E_{out}(0)|^2$, is $I_{m0} = I_m \exp(-d_p/2)$ or $I_{m0} =$

$I_m \exp(-d_p/F)$, where $I_m = |E_{\text{in}}(0)|^2$ is the maximum intensity of the input pulse and $F = 2$ is the finesse of the HFC. Thus, the maximum intensity of this pulse decreases according to the Beers' law, $I_{m0} = I_m \exp(-d_{\text{eff}})$, with increase of the effective optical thickness (optical depth) $d_{\text{eff}} = d_p/F$. This thickness is reduced F times with respect to the optical depth seen by the monochromatic radiation, which is tuned in the center of the absorption peak. This is because of transparency windows present in the spectrum.

The maximum intensity of the first pulse, delayed by time $t_1 = \pi/\nu_0$, is $I_{m1} = I_m(d_{\text{eff}}/2)^2 \exp(-d_{\text{eff}})$, where $I_{m1} = |E_{\text{out}}(t_1)|^2$. The intensity I_{m1} takes maximum value $I_{m1} = e^{-2}I_m = 0.135I_m$ when $d_{\text{eff}} = 2$ or $d_p = 4$. The maximum amplitude of the first pulse for this value of the effective thickness is $E_{m1}(t_1) = e^{-1}E_0 = 0.368E_0$, where $E_0 = E_{\text{in}}(0)$; see Fig. 2(b). Here and below, numbering of the pulse intensity I_{mk} and amplitude $E_{mk}(t_k)$ follows the number k in the pulse delay, $t_k = k\pi/\nu_0$.

The area of the output pulse train, shown in Fig. 2,

$$S_{\text{out}} = \int_{-\infty}^{+\infty} E_{\text{out}}(t) dt, \quad (16)$$

is conserved, $S_{\text{out}} = S_{\text{in}}$, (where S_{in} is the input pulse area) if the central frequency of the input pulse is tuned in the center of one of the transparency windows. For the input pulse, whose central frequency is tuned in resonance with one of the absorption peaks, the pulse-train area reduces as $S_{\text{out}} = S_{\text{in}} \exp(-d_{\text{eff}})$. These results follow from the ES (13) and (14) since

$$\sum_{k=0}^{+\infty} \frac{(\pm d_{\text{eff}}/2)^k}{k!} = e^{\pm d_{\text{eff}}/2}. \quad (17)$$

The time-integrated intensity of the output pulses,

$$\langle I_{\text{out}} \rangle_t = \int_{-\infty}^{+\infty} |E_{\text{out}}(t)|^2 dt, \quad (18)$$

decreases as

$$\langle I_{\text{out}} \rangle_t = e^{-d_{\text{eff}}} I_0(d_{\text{eff}}) \langle I_{\text{in}} \rangle_t, \quad (19)$$

irrespective of the pulse central frequency ω_c , since

$$\sum_{k=0}^{+\infty} \frac{(\pm d_{\text{eff}}/2)^{2k}}{(k!)^2} = I_0(d_{\text{eff}}), \quad (20)$$

where $\langle I_{\text{in}} \rangle_t$ is the time-integrated intensity of the input pulse and $I_0(x)$ is the modified Bessel function of zero order; see Ref. [27]. When $d_{\text{eff}} \geq 3.75$, Eq. (19) is approximated as

$$\langle I_{\text{out}} \rangle_t = \frac{0.4}{\sqrt{d_{\text{eff}}}} \langle I_{\text{in}} \rangle_t. \quad (21)$$

For $0 \leq d_{\text{eff}} \leq 3.75$, Eq. (19) is approximated by the expression

$$\langle I_{\text{out}} \rangle_t = (1 + 0.25d_{\text{eff}}^2 + 0.016d_{\text{eff}}^4 + 0.0004d_{\text{eff}}^6) e^{-d_{\text{eff}}} \langle I_{\text{in}} \rangle_t; \quad (22)$$

see Ref. [27]. A graphical illustration of the dependence (22) on d_{eff} is shown in Fig. 4.

If the effective thickness is large ($d_{\text{eff}} \gg 1$), the maximum amplitudes of the pulses form a bell-shaped envelope [see

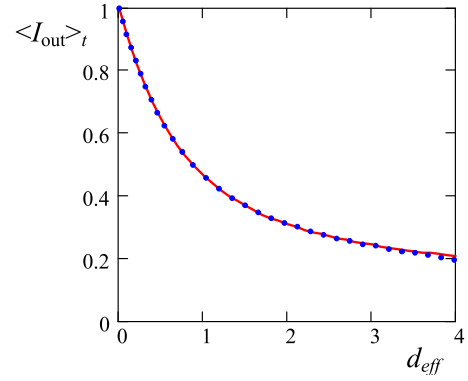


FIG. 4. Dependence of the time-integrated intensities of the pulses (net intensity) at the exit of HFC (normalized to $\langle I_{\text{in}} \rangle_t$) on effective thickness d_{eff} . The solid red line is the exact dependence, described by Eq. (19). The dotted blue line is the approximation, given by Eq. (22).

Fig. 2(d)]. The envelope can be described analytically if we use Stirling's formula for the factorial, which is

$$k! = \sqrt{2\pi} k^{k+1/2} e^{-k+\theta/12k}, \quad (23)$$

where $k > 0$ and $0 < \theta < 1$. This formula helps one to derive the approximate dependence of the maximum amplitude of the k th pulse, $E_{mk}(t_k)$, on k as

$$E_{mk}(t_k) = e^{-d_p/4} \frac{(d_p/4)^k}{k!} E_0 \approx e^{-d_p/4} \frac{(ed_p/4k)^k}{\sqrt{2\pi k}} E_0; \quad (24)$$

see Eq. (13). Taking into account that the k th pulse reaches its maximum amplitude at time $t_k = \pi k/\nu_0$, we express number k through time t_k , i.e., $k = \nu_0 t_k/\pi$, and obtain

$$E_{mk}(t_k) \approx e^{-d_p/4} \frac{(\pi ed_p/4\nu_0 t_k)^{\nu_0 t_k/\pi}}{\sqrt{2\nu_0 t_k}} E_0. \quad (25)$$

Then, we allow time t_k to evolve continuously in Eq. (25) and obtain the function $E_m(t)$, where index k is omitted. The plot of this function is shown in Fig. 2(d) by a dotted blue line. For large d_p , the function $E_m(t)$ clearly describes the net envelope of the pulse train. The maximum of this envelope takes place at time $t_{\text{max}} = \pi(d_p - 2)/4\nu_0$, which is found from the condition $\partial E_m(t)/\partial t = 0$. In the example, shown in Fig. 2(d) for $d_p = 30$, the envelope maximum is formed when $\nu_0 t_{\text{max}}/\pi = 7$.

For large d_{eff} , the maximum of the envelope, E_{max} , at time t_{max} , is described by equation

$$E_{\text{max}} = \sqrt{\frac{1}{\pi d_{\text{eff}} F(d_{\text{eff}})}} E_0, \quad (26)$$

where

$$F(d_{\text{eff}}) = e \left(1 - \frac{1}{d_{\text{eff}}}\right)^{d_{\text{eff}}}. \quad (27)$$

According to the notable special limit,

$$\lim_{d_{\text{eff}} \rightarrow +\infty} \left(1 - \frac{1}{d_{\text{eff}}}\right)^{d_{\text{eff}}} = e^{-1}, \quad (28)$$

the function $F(d_{\text{eff}})$ tends to 1. This function differs from 1 very little if $d_{\text{eff}} \geq 10$ [i.e., $F(10) = 0.891$] and takes values not very different from 1 for smaller d_{eff} . For example, we have $F(5) = 0.758$.

The half width at half maximum of the function $E_m(t)$ is found from the equation $E_m(t_{\text{max}} \pm t_{\text{hmax}}) = E_m(t_{\text{max}})/2$. Its solution gives the full width at half maximum $t_w = 2t_{\text{hmax}}$, which is approximated as

$$t_w = \frac{2\pi}{\nu_0} \sqrt{d_{\text{eff}} \ln(2)} \quad (29)$$

for large value of the optical thickness d_{eff} .

V. TIME-BIN QUBITS AND THEIR TOMOGRAPHY

Suppose that we have two harmonic frequency crystals with identical periods, ν_0 , and optical thicknesses, d_p , but the frequencies of their central transparency window $\omega_{\tau c}$ are differently displaced with respect to the central frequency of the incident pulse. In this section, we consider the case when the incident pulse contains only one photon.

At the exit of the first HFC, the probability amplitude of the radiation field is

$$|a_1\rangle = \sum_{k=0}^{+\infty} e^{i\pi k \delta_1 / \nu_0} c_k |b_k\rangle, \quad (30)$$

where $|b_k\rangle$ is a single-photon pulse centered at time $\pi k / \nu_0$, δ_1 is the frequency shift of the central transparency window of HFC with respect to the frequency of the incident single-photon pulse $|b_0\rangle$, and $c_k = e^{-d_p/4} (d_p/4)^k / k!$ is the probability amplitude of the k th photon state. The probability of the state $|a_1\rangle$ is described by the equation

$$\sum_{k=0}^{+\infty} c_k^2 = e^{-d_p/2} I_0(d_p/2), \quad (31)$$

whose functional dependence on the HFC thickness, d_p , is shown in Fig. 4; see Sec. IV.

We send state $|a_1\rangle$ to the second HFC whose shift of the central transparency window is δ_2 . To derive the resultant state $|a_2\rangle$, we turn to Eq. (9) for the Fourier transform of the radiation field passed through a single HFC, which helps to find that the field transmitted through two HFCs is described by

$$E_0(l, \nu) = E_0(0, \nu) \exp \left\{ -\frac{d_p}{2} + \frac{d_p}{4} e^{i\pi \nu / \nu_0} (e^{i\pi \delta_1 / \nu_0} + e^{i\pi \delta_2 / \nu_0}) \right\}. \quad (32)$$

Then, the photon state at the exit of the second HFC can be expressed as

$$|a_2\rangle = \sum_{k=0}^{+\infty} e^{i\pi k \delta_{\pm} / \nu_0} C_k |b_k\rangle, \quad (33)$$

where $C_k = (d_p/2)^k \cos^k(\pi \delta_{\pm} / \nu_0) e^{-d_p/2} / k!$ and $\delta_{\pm} = (\delta_1 \pm \delta_2)/2$. If $\delta_1 = \delta_2$, the probability of state $|a_2\rangle$ is $P_{\text{total}} = \sum_{k=0}^{+\infty} C_k^2 = e^{-d_p} I_0(d_p)$. When $\delta_2 = \delta_1 \pm \nu_0$, this probability is $\sum_{k=0}^{+\infty} C_k^2 = e^{-d_p}$. For a particular values of optical thickness

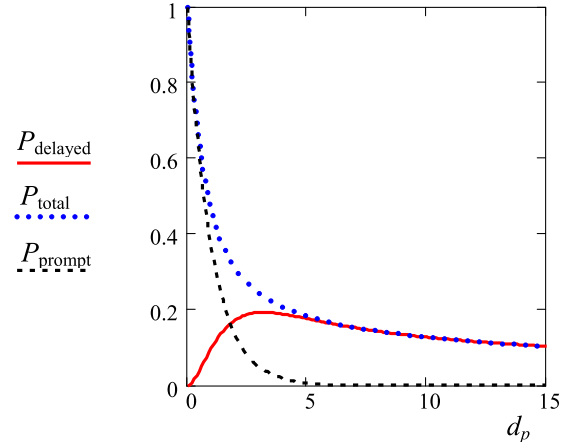


FIG. 5. Dependencies of the probabilities P_{total} (dotted blue line), P_{prompt} (dashed black line), and P_{delayed} (solid red line) on the optical thickness of the HFC, d_p .

d_p , these probabilities are very different. Actually, when $\delta_2 = \delta_1 \pm \nu_0$, the field at the exit of the second HFC contains only the prompt state $|b_0\rangle$ whose probability decreases as $P_{\text{prompt}} = C_0^2 = e^{-d_p}$, while on condition $\delta_1 = \delta_2$, all delayed states $|b_k\rangle$ are present. Their probability is described by the function $P_{\text{delayed}} = \sum_{k=1}^{+\infty} C_k^2 = e^{-d_p} [I_0(d_p) - 1]$. Dependencies of the probabilities P_{total} , P_{prompt} , and P_{delayed} on the optical thickness d_p are shown in Fig. 5. If, for example, we take optical thickness d_p of each HFC equal to 6, then we have that $P_{\text{prompt}} = 2.48 \times 10^{-3}$ and $P_{\text{delayed}} = 0.164$, which means that almost all of the radiation field is concentrated in the delayed photon states. The tomography of these states whose probability amplitudes depend on $\cos(\pi \delta_{\pm} / \nu_0)$ can be implemented as follows. For an arbitrary value of δ_{\pm} , the probability of state $|a_2\rangle$, $P(\delta_{\pm}, d_p) = \sum_{k=0}^{+\infty} C_k^2$, is $P(\delta_{\pm}, d_p) = e^{-d_p} I_0[d_p \cos(\pi \delta_{\pm} / \nu_0)]$. The dependence of this probability on δ_{\pm} for $d_p = 6$ is shown in Fig. 6, which demonstrates a large contrast between the probabilities for $\delta_{\pm} = n\nu_0$ and $\delta_{\pm} = (n + 1/2)\nu_0$, where n is a positive or negative integer. Thus, the phases of the probability amplitudes $e^{i\pi k \delta_1 / \nu_0} c_k$ of state $|a_1\rangle$, created by the first HFC, can be found by the second HFC whose detuning δ_2 is varied with respect to δ_1 .

To simplify the tomography, one can use a mirror at the exit of the first HFC and place the AOM on the way back of the photon to this HFC. Then the use of the second HFC is not necessary. Changing the frequency of the reflected photon, one can find the phases of the probability amplitude of state

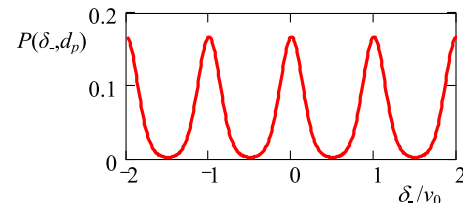


FIG. 6. Dependence of the detection probability of the photon, $P(\delta_{\pm}, d_p)$, transmitted through two HFCs with optical thickness $d_p = 6$ on the detuning of central frequencies of the HFCs, δ_{\pm} .

$|a_1\rangle$. Any phase shift acquired at the mirror and on the way back to the HFC will not affect the probability $P(\delta_-, d_p)$.

VI. ANHARMONIC FREQUENCY CRYSTAL

Another example of the atomic frequency comb is an anharmonic frequency crystal (AHFC). It has also a periodic structure in the absorption spectrum with a period $2\nu_0$, but many multiple frequencies $k\nu_0$ (where k is integer) contribute to the spectrum. Below we consider the crystal with the imaginary part of the susceptibility, which is described by the function

$$\chi''_{\text{ah}}(\nu) = \chi_0 \sin^{10}\left(\frac{\pi\nu}{2\nu_0}\right) = \frac{\chi_0}{2^5} \left[1 - \cos\left(\frac{\pi\nu}{\nu_0}\right)\right]^5. \quad (34)$$

Similar to the HFC, this periodic structure can also be created by a particular pulse sequence repeated many times; see the Appendix.

The real part of the susceptibility, $\chi'_{\text{ah}}(\nu)$, is found from the Kramers-Kronig relation, given by Eq. (4), which gives

$$\chi'_{\text{ah}}(\nu) = \frac{\chi_0}{2^9} \sum_{k=0}^4 (-1)^k C_{10}^k \sin\left[\frac{(5-k)\pi\nu}{\nu_0}\right], \quad (35)$$

where C_{10}^k is the binomial coefficient,

$$C_{10}^k = \frac{10!}{(10-k)!k!}. \quad (36)$$

This result follows from the binomial theorem,

$$\begin{aligned} \sin^{10}\left(\frac{\pi\nu}{2\nu_0}\right) &= \left(i \frac{e^{-i\pi\nu/2\nu_0} - e^{i\pi\nu/2\nu_0}}{2}\right)^{10} \\ &= -2^{-10} \sum_{k=0}^{10} (-1)^k C_{10}^k e^{i(5-k)\pi\nu/\nu_0}. \end{aligned} \quad (37)$$

Frequency dependencies of the absorption $\sim \chi''(\nu)$ and dispersion $\sim \chi'(\nu)$ of the anharmonic frequency crystal are shown in Fig. 7(a). The width at half maximum of the absorption peaks is 4.27 times smaller than the distance between them, which gives finesse $F = 4.27$.

The function describing the frequency dependence of the intensity attenuation of the monochromatic radiation, transmitted through this AHFC, which is $\mathcal{T}_{\text{int}}(\nu, d_p) = \exp[-d_p \chi''_{\text{ah}}(\nu)/\chi_0]$, is shown in Fig. 7(b) for $d_p = 4$. Even for this moderate value of thickness d_p , the absorption dips of this function are broadened and their centers are flattened compared with $\chi''(\nu)$.

The functions $\chi'(\nu)$ and $\chi''(\nu)$ have a periodic dependence on frequency ν with a period $2\nu_0$. However, according to Eqs. (35) and (37), in addition to the oscillations with frequency ν_0 , they also have contribution of the harmonics $2\nu_0$, $3\nu_0$, $4\nu_0$, and $5\nu_0$.

The complex dielectric constant in the exponent of Eq. (8) gives the following expression for the transmission function of the AHFC:

$$T_{\text{ah}}(\nu) = \frac{d_p}{2\chi_0} [\chi''_{\text{ah}}(\nu) - i\chi'_{\text{ah}}(\nu)], \quad (38)$$

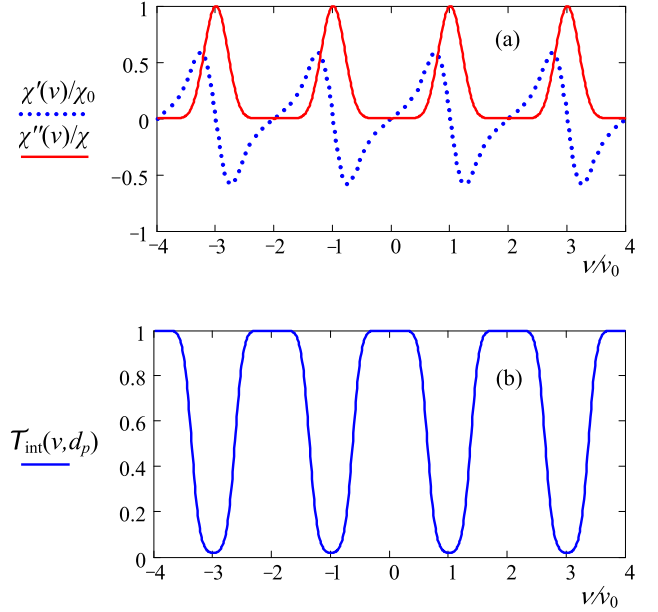


FIG. 7. (a) Absorption $\chi''(\nu)$ (red solid line) and dispersion $\chi'(\nu)$ (blue dotted line) components of the anharmonic frequency crystal, described by Eqs. (34) and (35). Both are normalized to χ_0 . (b) Frequency dependence of the intensity attenuation of the monochromatic radiation, transmitted through the AHFC with $d_p = 4$.

which can be expressed as

$$T_{\text{ah}}(\nu) = \frac{d_p}{2^{10}} \left[\frac{C_{10}^5}{2} + \sum_{k=1}^5 (-1)^k C_{10}^{5-k} e^{ik\pi\nu/\nu_0} \right]. \quad (39)$$

With the help of the expansion of the exponent in the equation

$$E_0(l, \nu) = E_0(0, \nu) \exp[-T_{\text{ah}}(\nu)], \quad (40)$$

in a power series of $T_{\text{ah}}(\nu)$ and inverse Fourier transformation, given by Eq. (12), one can derive the analytical time dependence of at least the first four pulses at the exit of the anharmonic frequency crystal, i.e.,

$$E_{\text{out}}(t) = e^{-\frac{63}{512}d_p} \sum_{k=0}^{\infty} e^{i\pi k\delta_s/\nu_0} A_k(d_p) E_{\text{in}}\left(t - \frac{\pi k}{\nu_0}\right), \quad (41)$$

where $A_0 = 1$, $A_1(d_p) = \frac{105}{512}d_p$, $A_2(d_p) = -\frac{15}{128}d_p + \frac{1}{2}\left(\frac{105}{512}\right)^2 d_p^2$, $A_3(d_p) = \frac{45}{1024}d_p - \frac{105}{512} \times \frac{15}{128}d_p^2 + \frac{1}{6}\left(\frac{105}{512}\right)^3 d_p^3, \dots$ Other parameters have the same meaning as for the HFC. A comparison of the time dependencies of the numerically calculated $E_{\text{out}}(t)$ with the help of Eqs. (12), (40), and the analytical approximation (41), where only the first four pulses are taken into account, is shown for $\delta_s = 0$ in Fig. 8. The coincidence for the first four pulses is excellent. The exact expression for the maximum amplitude of the pulse with no delay is $E_0 \exp(-63d_p/512)$, which gives $E_0 \exp(-d_p/2F_{\text{exc}})$, where $F_{\text{exc}} = 4.063$. This value is slightly smaller than finesse $F = 4.27$, estimated from the structure of the absorption spectrum.

The exact expression for the maximum amplitude of the first delayed pulse is $E_{m1} = E_0 A_1(d_p) \exp(-63d_p/512)$. Its

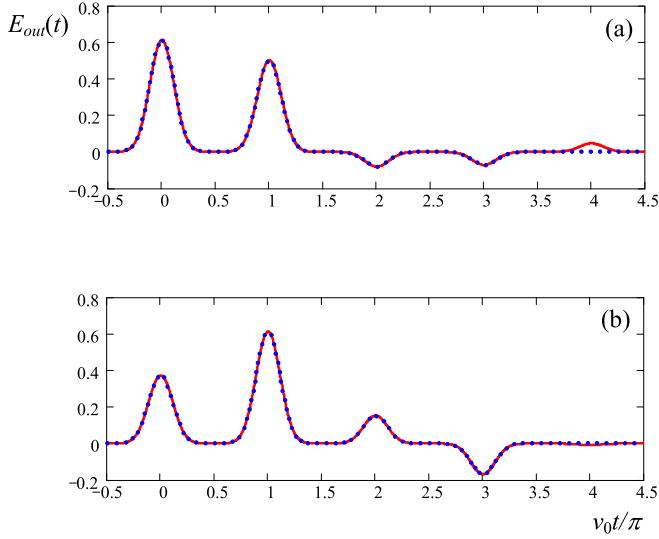


FIG. 8. Time dependence of the Gaussian pulse transmitted through the AHFC with optical thickness (a) $d_p = 4$ and (b) 8. Parameter r of the Gaussian pulse is $2\nu_0$ and $\delta_s = 0$. The solid red line corresponds to the numerical integration according to Eq. (12) with the transmission function, defined in Eqs. (39) and (40). The dotted blue line is plotted according to the analytical result, given in Eq. (41), where only the first four terms are taken into account. The pulse amplitude is normalized to the amplitude of the input pulse E_0 .

dependence on the optical thickness d_p is shown in Fig. 9. The maximum amplitude of this pulse, $0.613E_0$, is achieved when $63d_p/512 = 1$, which gives $d_p = 8.127$. For this value of thickness, we have $E_{m1} = \frac{105}{63} e^{-1} E_0 = 1.67 e^{-1} E_0$.

For the HFC, the maximum amplitude of the first delayed pulse is $E_{m1} = E_0(d_p/4) \exp(-d_p/4)$, whose global maximum $E_{m1} = e^{-1} E_0$ is achieved when $d_p = 4$. A comparison of the results for the HFC and AHFC shows that narrowing of the width of the absorption peaks with respect to the crystal period $2\nu_0$ increases the attainable maximum amplitude of the first delayed pulse. However, since finesse of the comb spectrum increases from $F = 2$ for the HFC to $F_{\text{exc}} = 4.063$ for the AHFC, the optical depth d_p providing maximum am-

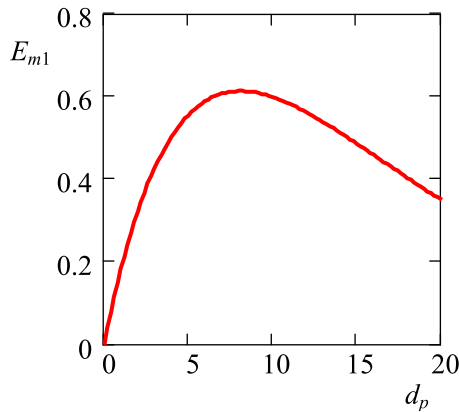


FIG. 9. Dependence of the maximum amplitude of the first delayed pulse (normalized to the amplitude of the input pulse E_0) on the optical thickness d_p .

plitude of the first delayed pulse must increase proportionally from $d_p = 4$ to $d_p = 8.127$.

VII. HOLE-BURNING TECHNIQUE

Frequency filters with a periodic spectrum could be realized, for example, with the help of the combination of the system of many minicavities interacting with a common broadband cavity coupled with the external waveguide [28,29]. However, the most common technique is the hole burning, which allows one to create a periodic sequence of the absorption lines and transparent windows in a wide inhomogeneously broadened absorption spectrum [8–12]. In the preparation stage, the periodic dependence of the population difference $n(\omega_A)$ of the ground and excited states on resonance frequency of atoms ω_A is created. Below, the real and imaginary parts of the atomic susceptibility are derived for the HFC and two types of AHFCs.

For a weak pulse, the linear response approximation (LRA) is applicable for the description of the density matrix evolution of atoms in the medium, $\rho_{mn}(z, t)$. The population change of the ground g and excited e states is neglected in LRA and only the equation for the nondiagonal element, $\rho_{eg}(z, t) = \sigma_{eg}(z, t) \exp(-i\omega_c t + ik_c z)$, is considered in the form

$$\frac{\partial}{\partial t} \sigma_{eg}(z, t) = (i\Delta - \gamma) \sigma_{eg}(z, t) + i\Omega(z, t)n(\Delta), \quad (42)$$

where ω_c and k_c are the frequency and the wave number of the input pulse, z is the propagation distance, counted from the input face of the medium inside, γ is the decay rate of the atomic coherence responsible for the homogeneous broadening of the absorption line, $\sigma_{eg}(t)$ is the slowly varying part of the nondiagonal element of the atomic density matrix, $\Delta = \omega_c - \omega_A$ is the difference of the frequency ω_c of the weak pulsed field and resonant frequency ω_A of an individual atom, $\Omega(t) = \mu_{eg} E_0(z, t)/2\hbar$ is the Rabi frequency, which is proportional to the time-varying field amplitude $E_0(z, t)$ and dipole-transition matrix element between g and e states, μ_{eg} , and $n(\Delta)$ is the long-lived population difference, created by the hole burning. If the atom is in the ground state, then $n(\Delta)$ is equal to unity. If the atom with the frequency $\omega_A = \omega_c - \Delta$ is removed by the hole burning to the shelving state, then $n(\Delta)$ is zero.

With the help of the Fourier transform, Eq. (42) is reduced to the algebraic equation whose solution is

$$\sigma_{eg}(z, \nu) = -\frac{\Omega(z, \nu)n(\Delta)}{\nu + \Delta + i\gamma}. \quad (43)$$

In the slowly varying amplitude approximation, the wave equation is reduced to

$$\widehat{L}E_0(z, t) = i\hbar\alpha_p\gamma\sigma_{eg}(z, t)/\mu_{eg}, \quad (44)$$

where $L = \partial_z + c^{-1}\partial_t$, $\alpha_p = 4\pi\omega_c N|\mu_{eg}|^2/\gamma\hbar c$ is the absorption coefficient, and N is the density of atoms. After Fourier transformation, the wave equation is reduced to

$$\left[\frac{\partial}{\partial z} - \frac{i\nu}{c} + A(\nu) \right] \Omega(z, \nu) = 0, \quad (45)$$

where

$$A(\nu) = \frac{i\alpha_p\gamma/2}{\nu + \Delta + i\gamma}. \quad (46)$$

The solution of Eq. (45),

$$E_0(z, \nu) = E_0(0, \nu) \exp[(i\nu z/c) - A(\nu)z], \quad (47)$$

coincides with Eq. (8).

Below, the HFC and two examples of AHFCs will be considered.

A. Harmonic frequency crystal

We consider the case when the population difference follows harmonic frequency dependence, i.e.,

$$n(\Delta) = \frac{1 - \cos(\pi\Delta/\nu_0)}{2}. \quad (48)$$

For simplicity, we suppose that before the hole burning, the frequency distribution of atoms was infinite and uniform. This assumption corresponds to a broad and flat inhomogeneous broadening, which is valid if the inhomogeneous width is much larger than the period $2\nu_0$. Then the averaged atomic coherence is

$$\langle\sigma_{eg}(\nu)\rangle_{\Delta} = \frac{1}{\pi\Gamma} \int_{-\infty}^{+\infty} \sigma_{eg}(\nu) d\Delta, \quad (49)$$

where Γ is the width of inhomogeneous broadening. This expression cannot be used to estimate the exact value of the optical thickness d_p since it does not contain the information about the width and shape of the initial inhomogeneous broadening and how the periodic structure in the absorption spectrum was created. However, it allows one to find the actual frequency dependencies of $\chi'(\nu)$, $\chi''(\nu)$ and derive the solutions (9) and (11) for the case of the hole burning.

Analytical calculation of the integral (49) within adopted approximation gives

$$\langle\sigma_{eg}(\nu)\rangle_{\Delta} = i \frac{\Omega(\nu)}{2\Gamma} (1 - e^{-\pi\gamma/\nu_0 + i\pi\nu/\nu_0}). \quad (50)$$

From this result, it follows that if the population difference has harmonic frequency dependence, given by Eq. (48), then the Fourier transform of the field at the exit of the medium is described by

$$E_0(l, \nu) = E_0(0, \nu) \exp \left\{ i\nu \frac{l}{c} - \frac{d_p}{4} + \frac{d_r}{4} e^{i\pi\nu/\nu_0} \right\}, \quad (51)$$

where $d_r = d_p \exp(-\pi\gamma/\nu_0)$; cf. Eq. (9). Thus, harmonic frequency dependence of the population difference results in a decrease of the parameter d_p to d_r in the expression for all the time-delayed pulses and does not affect the amplitude of the pulse with no delay, i.e.,

$$E_0(l, \nu) = E_{in}(\nu) e^{-d_p/4} \sum_{k=0}^{+\infty} \frac{(d_r/4)^k}{k!} e^{i\pi k\nu/\nu_0}. \quad (52)$$

If $\gamma \ll \nu_0$, this decrease is negligible.

B. Anharmonic frequency crystal I

For the anharmonic frequency crystal, considered in Sec. VI, the population difference has a frequency dependence,

$$n(\Delta) = \sin^{10}(\pi\Delta/\nu_0). \quad (53)$$

After averaging the atomic coherence in accord with Eq. (49), one obtains

$$\langle\sigma_{eg}(\nu)\rangle_{\Delta} = i \frac{\Omega(\nu)}{2^{10}\Gamma} \left[C_{10}^5 + 2 \sum_{k=1}^5 (-1)^k C_{10}^{5-k} e^{k\pi(i\nu-\gamma)/\nu_0} \right], \quad (54)$$

which gives

$$T_{ah}(\nu) = \frac{d_p}{2^{10}} \left[\frac{C_{10}^5}{2} + \sum_{k=1}^5 (-1)^k C_{10}^{5-k} e^{k\pi(i\nu-\gamma)/\nu_0} \right]. \quad (55)$$

This transmission function allows one to derive the time dependence of the field at the exit of the AHFC. Similar to the harmonic frequency crystal, the produced pulses are described by almost the same equation as in Sec. VI [see Eq. (41)], but with the reduced amplitudes of the delayed pulses, i.e., $A_1(d_p) = \frac{105}{512} d_r$, $A_2(d_p) = -\frac{15}{128} d_r + \frac{1}{2} \left(\frac{105}{512}\right)^2 d_r^2$, etc., since thickness d_p in these amplitudes decreases as $d_r = d_p \exp(-\pi\gamma/\nu_0)$.

C. Anharmonic frequency crystal II

In this section, a periodic structure of Lorentzian peaks is considered. It can be classified as the anharmonic frequency crystal or AHFC II. This structure is possible to construct by repumping a set of Lorentzian peaks into a broad absorption dip, created initially by the hole burning; see Refs. [10–12] where such an AFC was considered. For the numerical analysis, we consider the finite sequence of the Lorentzian peaks in the population difference, which is described by

$$n(\Delta) = \sum_{n=-101}^{100} \frac{\Gamma_L^2}{[\Delta + \nu_L(2n+1)]^2 + \Gamma_L^2}, \quad (56)$$

where Γ_L is a half width of the Lorentzian peak and $2\nu_L$ is a distance between two neighboring peaks. The limits in the sum are chosen such that the absorption peaks are symmetrically placed around the central transparency window.

Calculating the integral in Eq. (49), one obtains

$$\langle\sigma_{eg}(\nu)\rangle_{\Delta} = -\frac{\Omega(\nu)}{2\Gamma} \sum_{n=-101}^{100} \frac{\Gamma_L}{\nu - \nu_L(2n+1) + i(\Gamma_L + \gamma)}. \quad (57)$$

This result allows one to express the Fourier transform of the pulses at the exit of the medium as

$$E_0(l, \nu) = E_0(0, \nu) \exp[-T_L(\nu)], \quad (58)$$

where

$$T_L(\nu) = \frac{d_p}{2} \sum_{n=-101}^{100} \frac{i\Gamma_0}{\nu - \nu_L(2n+1) + i\Gamma_0}, \quad (59)$$

and $\Gamma_0 = \Gamma_L + \gamma$.

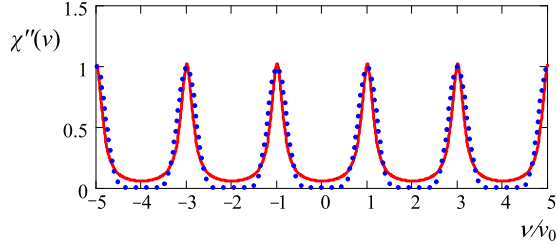


FIG. 10. Comparison of the absorption peaks, which are described by the imaginary part of the susceptibility, $\chi''(\nu)$, for the AHFC II consisting of the Lorentzian peaks (red solid line) and AHFC I described by the function $\sin^{10}(\pi \Delta/\nu_0)$ (dotted blue line). Absorption $\chi''(\nu)$ is normalized to χ_0 . The frequency dependencies are plotted for $\nu_L = \nu_0$ and $\Gamma_0 = 0.157\nu_L$.

To compare the AHFC consisting of the periodic sequence of the Lorentzian absorption peaks (AHFC II) with that considered in the previous section (AHFC I), we select such a value of Γ_0 when the absorption spectra of both are very similar. This condition is more or less satisfied when $\Gamma_0 = 0.157\nu_L$ and the period of both structures coincide, i.e., $\nu_0 = \nu_L$; see Fig. 10.

The time dependence of the field, $E_{\text{out}}(t)$, at the exit of the medium for the AHFC II is shown in Fig. 11. It is calculated numerically (solid red line) for the Gaussian input pulse with the help of the equation

$$E_{\text{out}}(t) = \frac{1}{2\pi} \int_{-\infty}^{+\infty} E_{\text{in}}(\nu) e^{-i\nu t - T_L(\nu)} d\nu. \quad (60)$$

Analysis of the numerical results shows that when $\Gamma_0 = 0.157\nu_L$ and $\nu_L = \nu_0$, the maximum amplitude of the pulse with no delay, E_{m0} , taking place at $t = 0$, has the same

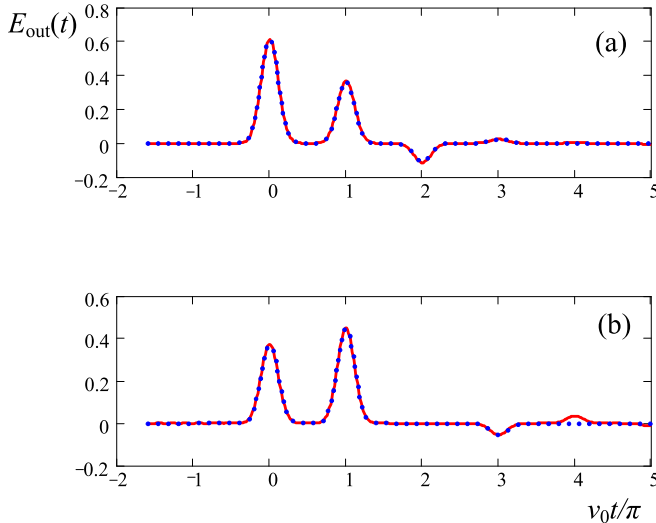


FIG. 11. Time dependence of the field $E_{\text{out}}(t)$ (normalized to E_0) at the exit of the medium for the AHFC II with (a) $d_p = 4$ and (b) 8 . The results, obtained by numerical integration in Eq. (60), are shown by a solid red line. Analytical results, which are described by Eq. (63), where $\delta_s = 0$ and only the first four terms in the sum are taken into account, are shown by a dotted blue line. Parameter r of the incident Gaussian pulse is $2\nu_0$.

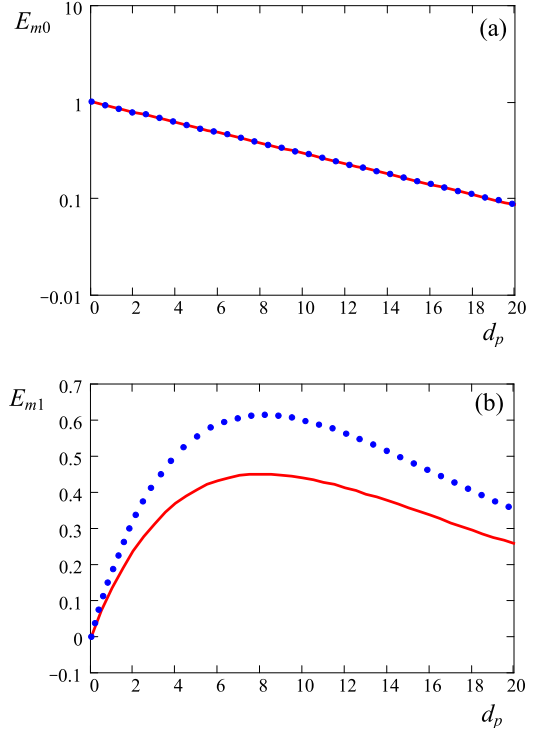


FIG. 12. Dependences of the maximum amplitude of (a) the pulse with no delay and (b) the first pulse with delay $t_{d1} = \pi/\nu_0$ on optical thickness d_p . The solid red line corresponds to AHFC II with $\Gamma_0 = 0.157\nu_L$, $\nu_L = \nu_0$ and the dotted blue line to AHFC I. The amplitude is normalized to E_0 .

dependence on the optical thickness d_p as for the AHFC I; see Fig. 12(a). This contradicts the finesse concept of the frequency combs, which predicts the amplitude $E_{m0} = E_0 \exp(-d_p/2F)$, where F is the comb finesse. For the AHFC I, the value F was estimated as $F_{\text{exc}} = 4.063$ (see Sec. VI), while for AHFC II, its finesse can be estimated as $\nu_L/\Gamma_0 = 6.37$, which is $\pi/2$ times larger than that following from the dependence E_{m0} on the optical thickness d_p , shown in Fig. 12(a) by a solid red line.

The maximum amplitude of the first delayed pulse, E_{m1} , is obtained for both AHFC I and AHFC II at the same value of the optical thickness, $d_p \simeq 8$; see Fig. 12(b). However, for AHFC II, this maximum is smaller. This difference could be explained by nonzero absorption at the center of the transmission windows due to the contribution of the Lorentzian wings of the absorption peaks; see Fig. 10. Remnant absorption at the centers of the transmission windows also reduces the amplitude of the pulse with no delay more than it is predicted by the exponent $\exp(-d_p/2F)$.

To estimate the amplitudes E_{m0} , E_{m1} of the first two pulses with no delay (t_0) and delayed (t_1), we express the transmission function as follows:

$$T_L(\nu) = \frac{d_p}{2} \sum_{k=0}^{+\infty} a_k e^{ik\pi\nu/\nu_L}, \quad (61)$$

where the coefficients in the sum are

$$a_k = \frac{1}{2\nu_0} \int_{-\nu_0}^{\nu_0} \frac{2}{d_p} T_L(\nu) e^{-ik\pi\nu/\nu_L} d\nu. \quad (62)$$

Then, the amplitude of the radiation field at the exit of the medium is described by

$$E_{\text{out}}(t) = e^{-a_0 d_p/2} \sum_{k=0}^{+\infty} (-1)^k B_k E_{\text{in}} \left(t - \frac{\pi k}{\nu_0} \right) e^{i\pi k \delta_s / \nu_0}, \quad (63)$$

where δ_s is a frequency shift of the central transparency window of AHFC II with respect to the frequency of the incident pulse, $B_0(d_p) = 1$, $B_1(d_p) = \frac{a_1 d_p}{2}$, $B_2(d_p) = \frac{1}{2} \left(\frac{a_1 d_p}{2} \right)^2 - \frac{a_2 d_p}{2}$, $B_3(d_p) = \frac{1}{6} \left(\frac{a_1 d_p}{2} \right)^3 - a_1 a_2 \left(\frac{d_p}{2} \right)^2 + \frac{a_3 d_p}{2}, \dots$

The coefficients a_k can be easily calculated. For example, for the infinite sum of Lorentzians [infinite sum in Eq. (59)], the coefficients are $a_0 = \frac{\pi \Gamma_0}{2\nu_L}$ and $a_k = (-1)^k \frac{\pi \Gamma_0}{\nu_L} e^{-k\pi \Gamma_0 / \nu_L}$, where $k = 1, 2, \dots$. If we introduce the effective thickness $d_{\text{eff}} = a_0 d_p = \frac{\pi \Gamma_0}{2\nu_L} d_p$, then the coefficients $B_k(d_p)$ can be expressed as $B_1(d_p) = -d_{\text{eff}} e^{-\Gamma_0 t_1}$, $B_2(d_p) = (d_{\text{eff}}^2 / 2 - d_{\text{eff}}) e^{-2\Gamma_0 t_1}$, $B_3(d_p) = -(d_{\text{eff}}^3 / 6 - d_{\text{eff}}^2 + d_{\text{eff}}) e^{-3\Gamma_0 t_1}$, where $t_k = k\pi / \nu_L$. Comparison of the results of the numerical integration of Eq. (60) with the analytical result of Eq. (63), where only the first four terms are taken into account and $\delta_s = 0$, is shown in Fig. 11. The coincidence of the results for the first four pulses is excellent.

Effective thickness gives us the value of the exact finesse, which is $F_{\text{exc}} = 2F/\pi$ if the finesse is estimated as $F = \nu_L / \Gamma_0$.

The structure of the solution (63) is such that the maximum amplitudes E_{km} of the pulses generated at times t_k are attenuated by the factor $\exp(-\Gamma_0 t_k)$. This makes a difference with a stimulated photon echo whose attenuation is described by the factor $\exp(-\gamma t_k)$, where $\gamma = 1/T_2$ is defined by the homogeneous dephasing time T_2 . In contrast to the stimulated photon echo, the pulses generated by AHFC II with a delay time t_k decay as $\exp(-t_k/T_2^*)$, where $T_2^* = 1/\Gamma_L$ can be considered as inhomogeneous dephasing time, which is defined by the half width of inhomogeneously broadened Lorentzian absorption peaks.

In the numerical example, shown in Fig. 11, the parameter characterizing the absorption peaks is $\Gamma_0 = 0.157\nu_L$. For this relation between Γ_0 and ν_L , one can find that for AHFC II, $a_0 = 0.246$ and $a_0 d_p / 2 = 0.123 d_p$, which coincides with the argument of the exponent for the prompt pulse in the solution for AHFC I, i.e., $63 d_p / 512 = 0.123 d_p$. Therefore, attenuation of the prompt pulse with increase of d_p , shown in Fig. 12(a), is the same for AHFC I and AHFC II if $\Gamma_0 = 0.157\nu_L$. Also, the coefficient $a_0 = 0.246$ gives the exact value of the finesse for this comb $F_{\text{exc}} = a_0^{-1}$ coinciding with the numerically found value 4.063.

The maximum amplitude of the first delayed pulse, E_{m1} , is achieved when $d_p = 2/a_0 = 4\nu_L / \Gamma_0$. For this value of the optical thickness d_p , we have

$$E_{m1} = -e^{-a_0 d_p/2} B_1(d_p) E_0 = 2e^{-1-\pi \Gamma_0 / \nu_L} E_0. \quad (64)$$

In the numerical example, shown in Fig. 12(b) for $\Gamma_0 = 0.157\nu_L$, the maximum amplitude of the first delayed pulse is achieved when $d_p = 2/a_0 = 8.13$. For this value of optical thickness, the amplitude E_{m1} is estimated as $E_0 e^{-1} (a_1/a_0) = 0.449 E_0$.

According to Eq. (64), the amplitude of the first pulse with a delay t_1 cannot be larger than 73.6% of the amplitude of

the input pulse since $2e^{-1} = 0.736$. This maximum amplitude is achieved if the condition $\pi \Gamma_0 / \nu_L \ll 1$ is satisfied. Since the optimal value of thickness is $d_p = 4\nu_L / \pi \Gamma_0$, we have $d_p \gg 1$. Thus, the maximum intensity of the first retrieved pulse, which is $4e^{-2} = 0.54$ of the intensity of the incident pulse, can be achieved only for an AFC with very narrow absorption peaks and large thickness satisfying the condition $d_p = 2/a_0 = 4\nu_L / \pi \Gamma_0$.

For the HFC, the maximum amplitude of the first delayed pulse is achieved when $d_p = 4$. Its value is $E_{m1} = e^{-1} E_0 = 0.368 E_0$, while intensity is $I_{m1} = e^{-2} I_0 = 0.135 I_0$, i.e., four times smaller than the maximum attainable intensity for AHFC II, which is $I_{m1} = 4e^{-2} I_0 = 0.54 I_0$ for very large values of d_p and finesse F . Meanwhile, if we take AHFC II with $d_p = 4$ and $\Gamma_0 = 0.157\nu_L$, which gives finesse $F = \nu_L / \Gamma_0 = 6.37$, we obtain the same maximum amplitude of the first delayed pulse $E_{m1} = 0.368 E_0$ as for the HFC with $d_p = 4$. Thus, a moderate value of optical thickness d_p does not allow one to achieve large amplitude E_{m1} and hence large efficiency of quantum memory based on the AFC.

In Ref. [11], the efficiency of the quantum memory based on the AFC, consisting of Lorentzian peaks, was calculated (see Eq. (2) in Ref. [11]). If we reconstruct from this efficiency the maximum amplitude of the first delayed pulse, we obtain

$$E_{m1} = d_p \tanh(\pi/2F) e^{-d_p \tanh(\pi/2F)/2 - \pi/F} E_0. \quad (65)$$

If finesse F of the AFC is defined according to Ref. [9] as $F = \nu_L / \Gamma_0$, then from this expression we can reconstruct the corresponding values of the coefficients a_0 and a_1 in the analytical solution, given by Eq. (63), which are $a_0 = \tanh(\pi \Gamma_0 / 2\nu_L)$ and $a_1 = -2 \tanh(\pi \Gamma_0 / 2\nu_L) e^{-\pi \Gamma_0 / \nu_L}$. For high finesse when $\nu_L \gg \Gamma_0$, these coefficients almost coincide with those calculated with the help of Eq. (62) for an infinite number of Lorentzian peaks. They are $a_0 = \pi \Gamma_0 / 2\nu_L$ and $a_1 = -(\pi \Gamma_0 / \nu_L) e^{-\pi \Gamma_0 / \nu_L}$.

If instead of infinite number of the Lorentzian peaks we take only two Lorentzians and calculate the integral in Eq. (62) for a_0 , we obtain

$$a_0 = \frac{\pi \Gamma_0}{2\nu_L} \left[1 - \frac{2}{\pi} \tan^{-1} \frac{\Gamma_0}{2\nu_L} \right]. \quad (66)$$

For large F , this function of $F = \nu_L / \Gamma_0$ almost coincides with function $a_0 = \tanh(\pi \Gamma_0 / 2\nu_L)$, derived in Ref. [11]. Their comparison is shown in Fig. 13.

It is interesting to note that a_0 , calculated for two Lorentzians, tends to 2, when $F \rightarrow 0$, while $a_0 = \tanh(\pi \Gamma_0 / 2\nu_L)$ tends to 1, and $a_0 = \pi \Gamma_0 / 2\nu_L$, calculated for infinite number of Lorentzians, tends to infinity. The limit $F \rightarrow 0$ corresponds to the case when spacing between Lorentzians tends to zero. Then one could expect that for two Lorentzians, a_0 in this limit must tend to 2, while for infinite number of Lorentzians, a_0 must tend to infinity. These arguments give a hint that $a_0 = \tanh(\pi \Gamma_0 / 2\nu_L)$ was calculated for a single Lorentzian in Ref. [11]. However, Lorentzian peaks have quite long wings of noticeable value for both $\chi''(\nu)$ and $\chi'(\nu)$. Therefore, calculating the coefficients a_0 and a_1 , one has to be careful in the estimation of the contribution of the neighboring Lorentzians wings to the integration interval $(-\nu_0, \nu_0)$ in Eq. (62). This is

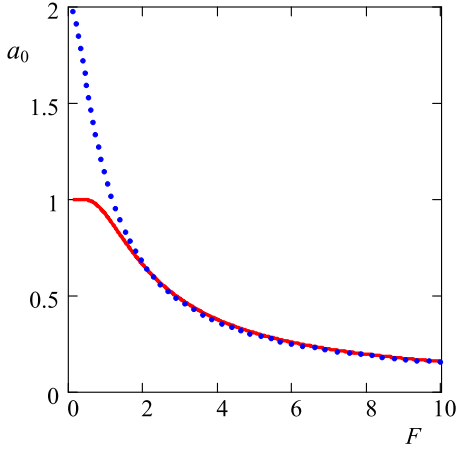


FIG. 13. Dependence of the coefficient a_0 on the finesse of the comb, consisting of Lorentzians, which is $F = \nu_L/\Gamma_0$. The solid red line corresponds to the result obtained in Ref. [11]. The dotted blue line is calculated for two Lorentzians.

especially important for moderate values of finesse. For example, for $F = 2$, the formula $a_0 = \tanh(\pi\Gamma_0/2\nu_L)$ gives $a_0 = 0.656$, while for infinite number of Lorentzians, we have $a_0 = 0.785$. The difference is as large as 20%. The same difference of 20% is present in the coefficients a_1 , calculated by formulae $a_1 = -2 \tanh(\pi\Gamma_0/2\nu_L)e^{-\pi\Gamma_0/\nu_L}$ and $a_1 = -(\pi\Gamma_0/\nu_L)e^{-\pi\Gamma_0/\nu_L}$. We can expect that this difference is the reason for the underestimation of the storage efficiency observed in experiments and reported in Ref. [10].

VIII. TIME-BIN QUBITS GENERATED BY AHFC II

In this section, we consider the generation of time-bin qubits by AHFC II. The state of the single-photon pulse transmitted through AHFC II can be expressed as follows:

$$|a_1\rangle = \sum_{k=0}^{+\infty} e^{i\pi k\delta_1/\nu_L} C_k |b_k\rangle, \quad (67)$$

where $C_k = (-1)^k B_k(d_p)e^{-a_0 d_p/2}$. Here and below, the notations are the same as in Secs. V and VII. We send state $|a_1\rangle$ to the second AHFC whose shift of the central transparency window is δ_2 . Then, the state at the exit of two crystals can be found with the help of the function

$$T_{\text{ah2}}(\nu) = d_p \sum_{k=0}^{+\infty} a_k \cos(\pi k\delta_-/\nu_L) e^{i\pi k(\nu+\delta_+)/\nu_L}, \quad (68)$$

which gives

$$|a_2\rangle = \sum_{k=0}^{+\infty} e^{i\pi k\delta_+/\nu_L} C_k |b_k\rangle. \quad (69)$$

The coefficients C_k are calculated following the solution given in Eq. (63). They are $C_0 = e^{-a_0 d_p}$, $C_1 = -a_1 d_p \cos(\pi\delta_-/\nu_L) C_0$, $C_2 = [\frac{(a_1 d_p)^2}{2} \cos^2(\pi\delta_-/\nu_L) - a_2 d_p \cos(2\pi\delta_-/\nu_L)] C_0$, $C_3 = [-\frac{(a_1 d_p)^3}{6} \cos^3(\pi\delta_-/\nu_L) + a_1 a_2 d_p^2 \cos(\pi\delta_-/\nu_L) \cos(2\pi\delta_-/\nu_L) - a_3 d_p \cos(3\pi\delta_-/\nu_L)] C_0, \dots$

When $\delta_- = 0$, we have the same state as $|a_1\rangle$, but obtained by the filtering through AHFC II of the double thickness $2d_p$. When $\delta_- = \nu_L/2$, the probability amplitudes C_1 and C_3

become zero, while $C_2 = a_2 d_p C_0$. This is a quite obvious result since with the assumption $\delta_- = \nu_L/2$, we form out of two AHFC II one of the same thickness d_p but with a reduced period, which becomes $\Delta_a = \nu_L$. Then, the first delayed pulse is generated at time $t_2 = 2\pi/\nu_L$, which is two times longer than $t_1 = \pi/\nu_L$. The amplitude of this pulse is proportional to a_2 , which is the Fourier transform of $T_L(\nu)$ with the exponent $e^{i2\pi k\nu/\nu_L}$. Therefore, this coefficient is reduced by a factor of $e^{-\pi\Gamma_0/\nu_L}$ compared to a_1 .

Such a filtering with the help of the second AHFC II or by use of the mirror and AOM could provide information about phases $e^{i\pi k\delta_1/\nu_L}$ of the components of state $|a_1\rangle$. This could be implemented if we detect photon only in a short-time window centered at t_1 . By changing δ_- , we will observe oscillation of a number of photon counts with large contrast.

IX. DISCUSSION

Time-bin states, discussed in Secs. V and VIII, are quantum states if they contain one photon or less distributed among their components (time bins). Detection of a single photon in one of the time bins secures that no photon can be detected in any other time bins of the state.

These quantum states have properties quite similar to the time-bin qubits considered in Refs. [14,15]. For example, filtering a single-photon pulse through AHFC II creates state $|a_1\rangle$ [see Eq. (67)], which can be approximated as consisting of two time bins, i.e.,

$$|a_1\rangle \approx C_0 |b_0\rangle + e^{i\pi\delta_1/\nu_L} C_1 |b_1\rangle, \quad (70)$$

where probability amplitudes of the other time bins, C_k , with $k > 1$, are neglected since for AHFC II they are small; see Fig. 11. Filtering this state through the second AHFC whose shift of the central transparency window is δ_2 can be considered as an interference phenomenon. For example, if $\delta_1 = 0$ and $\delta_2 = \nu_L$, a single pulse transmitted through the first AHFC is split into prompt $|b_0\rangle$ and delayed $|b_1\rangle$ pulses having the probability amplitudes C_0 and C_1 with the same phase as the input pulse. After filtering the state $|a_1\rangle$ through the second AHFC, each pulse in this state is split again into two, i.e., $C_0 |b_0\rangle$ is transformed into $C_0(C_0 |b_0\rangle - C_1 |b_1\rangle)$, and $C_1 |b_1\rangle$ is transformed into $C_1(C_0 |b_1\rangle - C_1 |b_2\rangle)$. The phase change by π of the delayed pulses is due to the frequency shift $\delta_2 = \nu_L$ of the second AHFC. The result of the interference of these states gives

$$|a_2\rangle = C_0^2 |b_0\rangle + 0 |b_1\rangle - C_1^2 |b_2\rangle, \quad (71)$$

where the probability amplitude of the state $|b_1\rangle$ becomes zero due to the interference of the prompt pulse transmitted through the second AHFC with the time delay T and the delayed pulse transmitted through the second AHFC with no delay. These pulses interfere destructively since they have opposite phases. For arbitrary values of the detunings δ_1 and δ_2 , the probability amplitude of the state $|b_1\rangle$ in $|a_2\rangle$ is $C_0 C_1 (e^{i\pi\delta_1/\nu_L} + e^{i\pi\delta_2/\nu_L})$.

It should be noted that actually the probability amplitude of the state $|b_2\rangle$ in Eq. (71) is not correct since in the derivation we did not take into account the presence of this state, created by the first AHFC, and transformation of the prompt pulse $|b_0\rangle$ to the state $|b_2\rangle$ in the second AHFC. Simple consideration

of these processes gives the correct value of this probability amplitude, which is $2C_0C_2 - C_1^2$.

In general, it is easy to vary the phase $\pi\delta_1/\nu_L$ gained by the photon between the two time bins in the state $|a_1\rangle$ by the AOM, while it is much more difficult to vary the amplitudes C_0 and C_1 , which are fixed for a given AHFC. Therefore, state $|a_1\rangle$ covers only a subset of all possible qubits. To simplify operations with this quantum state, it is preferable to create state $|a_1\rangle$ with $|C_1| = |C_2|$. For AHFC II, such a state is produced if the finesse of the comb $F = \nu_L/\Gamma_0$ is equal to π and optical thickness d_p is 5.4. Then we have $|C_1| = |C_2| = 0.257$.

The AHFC is capable to substitute interferometers in the protocol producing pulsed energy-time entangled twin photons, which was proposed and implemented in Ref. [14]. If we have two AHFCs with identical frequency periods, finesse, and optical thickness but having different central frequencies, i.e., one is centered at the frequency of the pump laser and another is centered at a half of this frequency, then the first AHFC splits the pump pulse into two pulses, prompt p_p and delayed p_d , which propagate through the nonlinear crystal where degenerate twin photons are created by spontaneous parametric down-conversion. Each photon from the pump laser, split in two parts, is transformed into twin photons, i.e., p_p into s_p and i_p , and p_d into s_d and i_d . Here, s and i mean signal and idle photons, respectively, and indexes p and d mean prompt and delayed photons. Then, these twin photons are sent to the analyzer, which is the second AHFC with central frequency equal to the frequency of the twin photons. We consider particular paths or time of arrival to the detectors, which are $s_p \rightarrow s_{pd}$, $i_p \rightarrow i_{pd}$, $s_d \rightarrow s_{dp}$, and $i_d \rightarrow i_{dp}$, where index pd means that the prompt twin photon is transmitted with a time delay and dp means that the delayed photon is transmitted without time delay through the second AHFC. Since these quantum paths are indistinguishable, one can observe two-photon interference in the photon coincidence-count measurements.

Comb structures of arbitrary shapes in the transmission spectra can be created experimentally by persistent hole burning in the absorption spectrum of organic molecules doped in a polymer matrix. These structures have almost infinite lifetime at liquid-helium temperature [30,31].

X. CONCLUSION

The propagation of light pulse in a medium with the periodic structure in the absorption spectrum is analyzed. Two periodic structures, harmonic and anharmonic, are considered. Both are idealized as having an infinite spectrum consisting of absorption peaks separated by transparency windows. Frequency-dependent complex dielectric constants are derived for these periodic structures with the help of the Kramers-Kronig relation and solution of the Bloch equations. The method of solution of the Maxwell-Bloch equation describing the pulse propagation in the frequency periodic medium (frequency crystal) is proposed. For the harmonic frequency crystal, the exact solution is obtained in a simple form. For the anharmonic frequency crystal, a simple analytical solution describing the first four pulses in the pulse sequence at the exit of the crystal is derived. Filtering a short

pulse through the harmonic frequency crystal allows one to generate a pulse sequence separated by long-time intervals. These pulses are coherent and could be applied to create time-bin qubits since the phases and amplitudes of the pulses can be manipulated by adjusting the parameters of the frequency crystal. Tomography of time-bin qubits is proposed. The HFC and AHFC can be created in the inhomogeneously broadened absorption spectrum of crystals with rare-earth-metal impurity ions by the hole-burning technique or by constructing the system of many mini- or microcavities interacting with a common broadband cavity coupled with an external waveguide.

ACKNOWLEDGMENTS

The author expresses his thanks to Prof. Lenar Tagirov for useful discussions and help in the manuscript preparation. This work was partially funded by the Program of Russian Academy of Sciences "Actual problems of the low temperature physics" and the Program of Competitive Growth of Kazan Federal University funded by the Russian Government.

APPENDIX

In [25] [see Eq. (5) in the reference], it is shown that pumping by pulse pairs,

$$E_{\text{pair}}(t) = E_p(t) + E_p(t - T), \quad (\text{A1})$$

where $E_p(t)$ is a short $\delta(t)$ -like pulse, in the medium with inhomogeneously broadened absorption spectrum and long lifetime of the excited state, creates the absorption and/or transmission profile, which is described by the function proportional to $1 + \cos(\nu T)$. This is because the Fourier transform of the pulse pair is

$$E_{\text{pair}}(\nu) = E_p(\nu) + E_p(\nu)e^{i\nu T}, \quad (\text{A2})$$

or $E_{\text{pair}}(\nu) = 2e^{i\nu T/2} \cos(\nu T/2)$; see Eq. (6) in Ref. [25]. Since the change of the population difference of the atomic states in the medium is proportional to the radiation intensity, $I_{\text{pair}}(\nu) = E_{\text{pair}}(\nu)E_{\text{pair}}^*(\nu)$ (see Eq. (4) in Ref. [25]), which is $I_{\text{pair}}(\nu) = 4I_0(\nu) \cos^2(\nu T/2) = 2I_p(\nu)[1 + \cos(\nu T)]$, the frequency grating in the atomic population, $n(\Delta) \sim 1 + \cos(\Delta T)$, is created by such a pulse pair. Here, $I_p(\nu) = |E_p(\nu)|^2$ is the intensity of the individual pulse. The center of the grating contains the absorption peak. If we detune from the center to the nearest dip in the absorption spectrum, $\Delta_s = \Delta + \pi/T$, then $n(\Delta_s) \sim 1 - \cos(\Delta_s T)$, which coincides with a structure inherent to the HFC with $\nu_0 = \pi/T$.

It is possible also to create AHFC I by the sequence of weak pulses repeated many times. For example, six pulses,

$$E_6(t) = \frac{E_p(t - \frac{5T}{2})}{10} + \frac{E_p(t - \frac{3T}{2})}{2} + E_p\left(t - \frac{T}{2}\right) + E_p\left(t + \frac{T}{2}\right) + \frac{E_p(t + \frac{3T}{2})}{2} + \frac{E_p(t + \frac{5T}{2})}{10}, \quad (\text{A3})$$

have the spectrum, which is

$$E_6(\nu) = \frac{16}{5} E_p(\nu) \cos^5\left(\frac{\nu T}{2}\right). \quad (\text{A4})$$

The power spectrum of this pulse sequence is

$$I_6(\nu) = \left(\frac{16}{5}\right)^2 I_p(\nu) \cos^{10}\left(\frac{\nu T}{2}\right). \quad (\text{A5})$$

Thus, such a pulse sequence is capable to produce the population grating $n(\Delta) \sim \sin^{10}(\Delta T/2)$, which gives $\chi''_{\text{ah}}(\nu) \sim \sin^{10}(\pi \nu/2\nu_0)$.

-
- [1] F. Wilczek, *Phys. Rev. Lett.* **109**, 160401 (2012).
- [2] K. Sacha, *Phys. Rev. A* **91**, 033617 (2015).
- [3] V. Khemani, A. Lazarides, R. Moessner, and S. L. Sondhi, *Phys. Rev. Lett.* **116**, 250401 (2016).
- [4] D. V. Else, B. Bauer, and C. Nayak, *Phys. Rev. Lett.* **117**, 090402 (2016).
- [5] C. W. von Keyserlingk, V. Khemani, and S. L. Sondhi, *Phys. Rev. B* **94**, 085112 (2016).
- [6] N. Y. Yao, A. C. Potter, I.-D. Potirniche, and A. Vishwanath, *Phys. Rev. Lett.* **118**, 030401 (2017).
- [7] S. Choi *et al.*, *Nature* **543**, 221 (2017).
- [8] H. de Riedmatten, M. Afzelius, M. U. Staudt, C. Simon, and N. Gisin, *Nature (London)* **456**, 773 (2008).
- [9] M. Afzelius, C. Simon, H. de Riedmatten, and N. Gisin, *Phys. Rev. A* **79**, 052329 (2009).
- [10] M. Bonarota, J. Ruggiero, J.-L. Le Gouët, and T. Chanelière, *Phys. Rev. A* **81**, 033803 (2010).
- [11] T. Chanelière, J. Ruggiero, M. Bonarota, M. Afzelius, and J.-L. Le Gouët, *New J. Phys.* **12**, 023025 (2010).
- [12] M. Bonarota, J.-L. Le Gouët, S. A. Moiseev, and T. Chanelière, *J. Phys. B* **45**, 124002 (2012).
- [13] N. Gisin, G. Ribordy, W. Tittel, and H. Zbinden, *Rev. Mod. Phys.* **74**, 145 (2002).
- [14] J. Brendel, N. Gisin, W. Tittel, and H. Zbinden, *Phys. Rev. Lett.* **82**, 2594 (1999).
- [15] I. Marcikic, H. de Riedmatten, W. Tittel, V. Scarani, H. Zbinden, and N. Gisin, *Phys. Rev. A* **66**, 062308 (2002).
- [16] R. T. Thew, A. Acin, H. Zbinden, and N. Gisin, *Phys. Rev. Lett.* **93**, 010503 (2004).
- [17] P. C. Humphreys, B. J. Metcalf, J. B. Spring, M. Moore, X.-M. Jin, M. Barbieri, W. S. Kolthammer, and I. A. Walmsley, *Phys. Rev. Lett.* **111**, 150501 (2013).
- [18] J. M. Donohue, M. Agnew, J. Lavoie, and K. J. Resch, *Phys. Rev. Lett.* **111**, 153602 (2013).
- [19] B. R. Nisbet-Jones, J. Dille, A. Holleczek, O. Barter, and A. Kuhn, *New J. Phys.* **15**, 053007 (2013).
- [20] F. Vagizov, V. Antonov, Y. V. Radeonychev, R. N. Shakhmuratov, and O. Kocharovskaya, *Nature (London)* **508**, 80 (2014).
- [21] R. N. Shakhmuratov, F. G. Vagizov, V. A. Antonov, Y. V. Radeonychev, M. O. Scully, and O. Kocharovskaya, *Phys. Rev. A* **92**, 023836 (2015).
- [22] R. N. Shakhmuratov, *Phys. Rev. A* **95**, 033805 (2017).
- [23] D. L. McAuslan, L. R. Taylor, and J. J. Longdella, *Appl. Phys. Lett.* **101**, 191112 (2012).
- [24] N. Horiuchi, *Nat. Photon.* **7**, 85 (2013).
- [25] H. Sönajalg and P. Saari, *J. Opt. Soc. Am. B* **11**, 372 (1994).
- [26] M. D. Crisp, *Phys. Rev. A* **1**, 1604 (1970).
- [27] *Handbook of Mathematical Functions*, edited by M. Abramowitz and I. A. Stegun (Dover, New York, 1965).
- [28] S. A. Moiseev, F. F. Gubaidullin, R. S. Kirillov, R. R. Latypov, N. S. Perminov, K. V. Petrovnin, and O. N. Sherstyukov, *Phys. Rev. A* **95**, 012338 (2017).
- [29] S. A. Moiseev, K. I. Gerasimov, R. R. Latypov, N. S. Perminov, K. V. Petrovnin, and O. N. Sherstyukov, *Sci. Rep.* **8**, 3982 (2018).
- [30] H. Schwerer, D. Erni, and A. Rebane, *J. Opt. Soc. Am. B* **12**, 1083 (1995).
- [31] A. Renn, U. P. Wild, and A. Rebane, *J. Phys. Chem.* **106**, 3045 (2002).